EURASTROS capsule design and re-entry analysis

Pascal Marquardt[1], Markus Fertig[2], Thomas Reimer[3], Ali Gülhan[4]
German Aerospace Center (DLR e.V.), Germany

Abstract

In this study, the capsule of the EURASTROS study is discussed in terms of its aerodynamic and aero-thermal properties, re-entry characteristics, structural design, and thermal protection system. Approximative methods are used to estimate the aerodynamic coefficients for the computation of nominal and off-nominal re-entry trajectories and to determine the nominal location of the center of gravity for statically stable flight. The re-entry trajectories are used to define the maximum mechanical and thermal loads on the capsule. The structure of the capsule is investigated by finite element analysis to determine the structural mass. Detailed Reynolds-averaged Navier-Stokes simulations are performed for three maximum load cases and the resulting heat flux distribution is used for the design of the thermal protection system. For this, recession and thermal insulation are considered.

1. Introduction

The EURASTROS study was a joint study between Ariane Group GmbH and German Aerospace Center (DLR), exploring the astronautic transport capabilities of Ariane 6. An overview of the study is given in [4]. The study included preliminary design of a crew module (CM), a service module (SM) [11], a launch abort system concept (LAS) with end-to-end abort capability [1], and a cost analysis [2]. The crew module is a capsule design derived from the Apollo capsule reduced in volume by 28% that can accommodate up to three astronauts. The main driver of the design choice is the fast and cost-effective development of the capsule due to heritage of the Atmospheric Reentry Demonstrator (ARD) and the existing databases of the Apollo program. The lift-off mass of the capsule is approximately 5000 kg.

In section 2, approximate methods were used to evaluate acceptable locations of the center of gravity for statically stable flight at a target hypersonic trim angle of attack. Furthermore, an aerodynamic database was generated using the same approach. In section 3, the aerodynamic coefficients were used to analyze the trajectory of the capsule for nominal and off-nominal re-entry as well as for launch abort to identify critical trajectory points for the design of the capsule. These design points define the maximum loads in terms of heat flux, dynamic pressure, and acceleration. The points are identified by analyzing return scenarios for ISS return and launch abort for controlled and uncontrolled/ballistic re-entry. A detailed analysis of the ascent trajectory and the resulting atmospheric and exo-atmospheric abort trajectories is presented in [1].

In section 4, high resolution, steady-state, 3-dimensional computational fluid dynamics (CFD) simulations including real gas effects and chemical nonequilibrium have been carried out to determine the heat flux distribution on the front and back shell of the capsule at the critical trajectory points and to cross validate the aerodynamic database. For the simulations, the CFD solver TAU [6] was used. The computational grid comprises a structured grid layer to allow for the determination of the surface heat flux with high accuracy. The normal resolution of the grid on the capsule surface is of the order of the local mean free path length. Furthermore, the grid is adaptively refined to accurately capture the Mach number and pressure gradients in the flow field, e.g., the bow shock. Turbulent flow and chemical equilibrium are assumed for the simulations at peak dynamic pressure. The points of maximum heat flux occur at much higher Mach number and altitude such that laminar flow and chemical non-equilibrium is considered.

For the TPS design, in section 5, the ablator material ZURAM® was selected as baseline which has been developed by DLR and is comparable in properties and performance to materials like PICA and ASTERM. For the TPS sizing, the total recession of the ablator material and the thermal insulation of the TPS material were analyzed. A transient thermal finite element method (FEM) simulation identified the thermal insulation as the main driver for the TPS sizing. The structure of the capsule is designed as a highly integrated metallic structure consisting of a cylindrical part with horizontal floor and a conical part on top, reinforced with orthogrid stiffeners on the outside of the pressure vessel.

---

[1] Supersonic and Hypersonic Technologies Department in Cologne: pascal.marquardt@dlr.de
[2] Spacecraft Department in Braunschweig
[3] Space System Integration Department in Stuttgart
[4] Supersonic and Hypersonic Technologies Department in Cologne, EURASTROS project manager at DLR

Two load cases, i.e., pressure difference between capsule internal and outside vacuum, and deceleration load during reentry, were investigated via FEM. The analysis results showed that the differential pressure load case is the dominating one for the assumptions made. Preliminary thickness values and masses for TPS and structure were determined.

2. Capsule Aerodynamics and Stability

The shape of the astronaut capsule is derived from the Apollo capsule, i.e., it has a spherical nose and a truncated conical back shell. To accommodate at least two astronauts, an outer diameter of $d = 3.5$ m is chosen which results in a volume of 11.6 m³ or about 72% of the Apollo capsule volume. A third astronaut can be accommodated as an option. The choice of the Apollo shape is beneficial for a fast and cost-efficient development of the capsule due to the heritage of the Atmospheric Reentry Demonstrator (ARD), which successfully flew in 1998 [13]. The outer shape of the capsule with its major dimensions is shown in Figure 1.
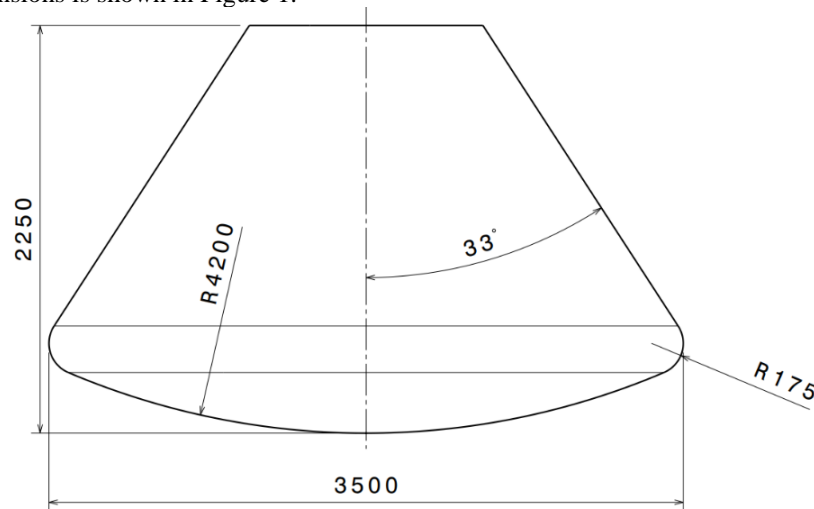

Figure 1: Outer shape of the EURASTROS capsule with its major dimensions.

The lift-off mass of the capsule is estimated as 5016 kg including the ISS docking adapter. Mass estimates for the structure and the TPS are based on the structural und TPS design which is discussed later. Masses of the subsystems, e.g., avionics, propulsion, etc., stem from an earlier study [12] and are scaled appropriately. The aerothermal loads of the capsule were studied in detail. Approximative methods were used to evaluate acceptable locations of the center of gravity to obtain a target hypersonic trim angle of 25°. Furthermore, an aerodynamic database was generated using the same approach. The aerodynamic coefficients were used to analyze the trajectory of the capsule for nominal and off-nominal re-entry as well as for launch abort scenarios. The results of the aerodynamic and stability analyses are discussed in section 6.2.1. Critical design points are analyzed by more accurate, high resolution techniques. These design points define the maximum loads in terms of heat flux density, dynamic pressure, acceleration, and total heat load. The points are identified by analyzing return scenarios for ISS return and launch abort at different altitudes for controlled and uncontrolled/ballistic re-entry. The detailed aerothermal analysis is carried out in section 4. The aerothermal loads are then used for the design of the thermal protection system (TPS) und the capsule structure which is described in section 5.

To analyze capsule re-entry trajectories, lift and drag coefficients of the capsule must be known. Furthermore, the moment coefficient is needed to determine at which angle of attack the capsule is oriented during re-entry and the stability derivative is necessary to judge if the capsule will keep its trim angle or gets unstable. An approximative method for the aerodynamic properties, namely the modified Newton method, is used to efficiently analyze the capsule aerodynamics without utilizing excessive computational resources or wind tunnel tests. For this, the capsule surface is discretized in approx. 480000 triangles. The aerodynamic properties of the capsule were studied for a range of locations of the center of gravity (COG) to investigate the influence of the COG location on the capsule and to find a reasonable COG location that gives beneficial re-entry properties. A feasible estimate for the axial COG location, based on values of the Orion capsule, is $0.26\,d = 0.91$ m behind the nose. For this COG location, the lateral COG shift as a function of the trim angle and the corresponding aerodynamic properties, i.e., lift-to-drag ratio c_L/c_D, ballistic coefficient BC, and static stability derivative $c_{m\alpha}$ are shown in Figure 2. A trim angle of 25° is chosen as baseline, in close agreement to the trim angle of the Apollo capsule. While a higher trim angle would lead to a higher lift-to-drag ratio, i.e., better maneuverability and larger cross range, the ballistic coefficient also increases rapidly with higher trim angles. This causes higher thermal loads during re-entry, demanding better TPS. Furthermore, trim angles above 33° would directly

expose the back shell to the freestream. To achieve the desired trim angle of 25°, the COG has to be shifted off-axis by $z_{COG} = 144.3$ mm. The resulting aerodynamic properties of the capsule for stable hypersonic flight are $c_L / c_D = 0.383$, $c_D = 1.25$, and $BC = 417$ kg/m². The coefficients are within 4% of the high-resolution simulations that are discussed in section 4.
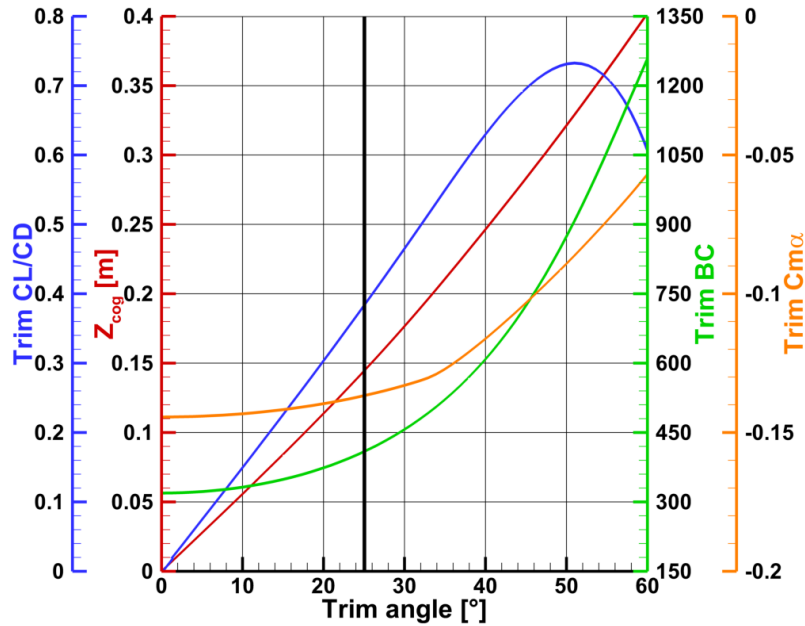

Figure 2: Lateral COG shift z_{COG}, lift-to-drag ratio c_L/c_D, ballistic coefficient BC, and stability derivative $c_{m\alpha}$ over trim angle for $x_{COG} = -0.91$ m.

For the structural design, the maximum mechanical loads on the capsule must be known. They occur at the point of maximum dynamic pressure during re-entry. The dynamic pressure for ballistic re-entry is much higher compared to nominal, lifting re-entry. The maximum value is found for ballistic re-entry after a high altitude launch abort. An in-depth analysis of high altitude launch abort of the EURASTROS configuration is given in [1]. For the definition of the maximum re-entry loads, a generic abort case was defined that is independent of the launch trajectory. It is defined as an abort at an altitude of 250 km at a velocity of 4174 m/s with 0° flight path angle that leads to re-entry loads slightly below the NASA g-load threshold for emergency returns [10]. For this worst survivable case, the peak g-load is $21.8g$ and the peak dynamic pressure is 88 kPa. The analysis of the pressure distribution on the capsule for this condition is shown in Figure 3. The highest local pressure on the heat shield is 163 kPa. The pressure distribution is used for dimensioning the structure of the capsule.
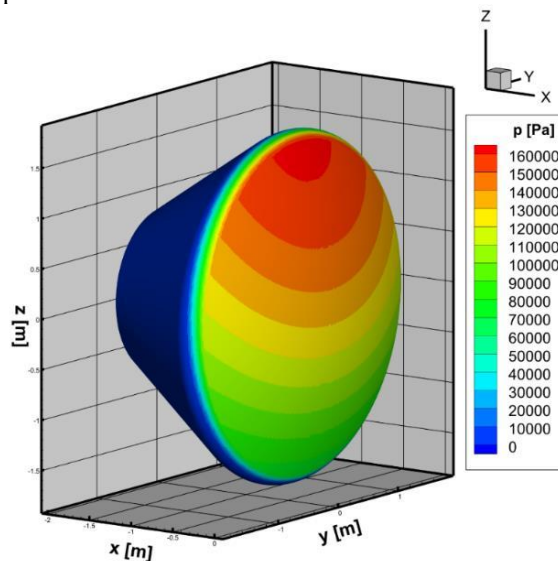

Figure 3: Pressure distribution for ballistic re-entry after launch abort ($H = 27.5$ km, $Ma = 8.6$, $\alpha = 25°$).

Marquardt, Fertig, Reimer, Gülhan

3. Re-entry analysis

The descent trajectory from the ISS has been analyzed to determine the loads on the capsule and to investigate the steering capability. Due to the off-axis center of gravity, the capsule is oriented at an angle of attack during re-entry which generates a lifting force. The bank angle of the capsule determines the direction in which the force is oriented. At 0° bank angle, the lift is directed upwards leading to a shallower re-entry with reduced loads and increased down range. When the capsule bank angle is changed, the lifting force is partially directed sideways which allows to steer the lateral course of the capsule, providing cross range. However, the vertical component of the lifting force gets smaller, which leads to a steeper re-entry, higher loads, and a shorter down range. By periodically reversing the direction of the bank angle, the effective lift, and hence, the slope of the trajectory, can be reduced without impacting the lateral course. Therefore, the down range and cross range of the capsule can be controlled to target a specific splashdown location. As a backup for emergencies, e.g., when the guidance and navigation system fail, a constant spin of the capsule of approx. 25°/s effectively cancels out the lifting force which leads to an uncontrolled, ballistic re-entry [7].

In the analysis, the ISS is assumed at its maximum altitude of 480 km. The de-orbit burn is carried out to pass the re-entry interface at 100 km with a flight path angle of -1.5°. The trajectories target a splashdown in the Atlantic Ocean off the west coast of Africa. In Figure 6, re-entry trajectories are shown for lifting entries with 0°, and ±45° in bank angle, and for ballistic re-entry. With maximum lift, i.e., 0° bank angle, the thermal and structural loads on the capsule are minimal. However, the re-entry is stretched over a longer duration which leads to higher integral heat loads compared to re-entry with lower lift. For a ballistic re-entry, the astronauts experience up to 8g whereas a re-entry with maximum lift only shows 2g. Nevertheless, all trajectories are within the limits defined by NASA for the commercial crew program [10] since the duration of the high g-loads is short enough. The small differences between positive and negative 45° bank angles arise from the rotation of the earth. The points of peak heat flux and peak dynamic pressure for lifting return from ISS with 0° bank angle, and the point of peak heat flux for ballistic ISS return are selected for detailed analysis by CFD and the corresponding conditions are summarized in Table 1.
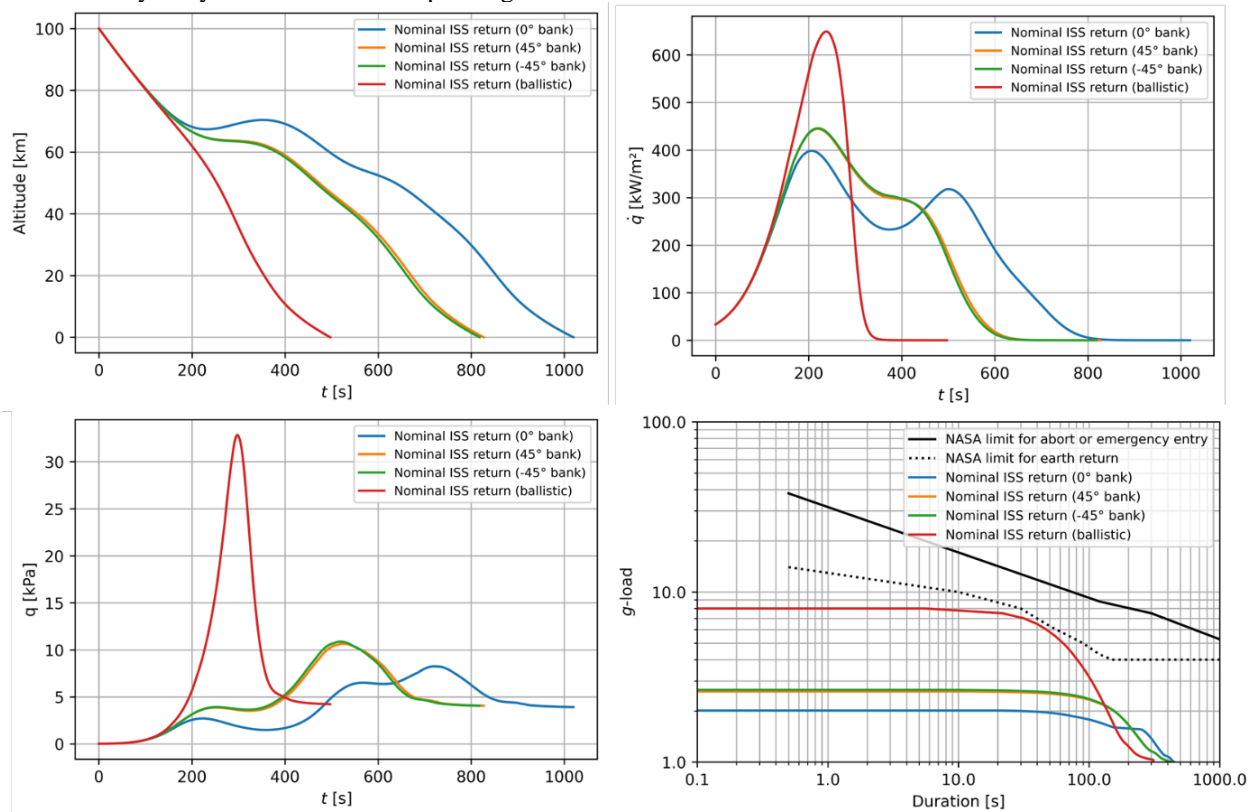

Figure 4: Nominal re-entry trajectory for ISS return with 0°/±45° bank angle and off-nominal uncontrolled/ballistic return.

In Figure 5, the cross range of the investigated trajectories is shown. Cross and down range are defined relative to earth surface. The asymmetry and non-zero cross range for the 0° bank angle and ballistic cases are due to earth rotation. The solid black line shows the splashdown cross and down range for a bank angle range from -90° to 90°. It is shown, that the capsule can be steered over a large range. With full lift, the reachable area is 472 km wide and 2369 km long.
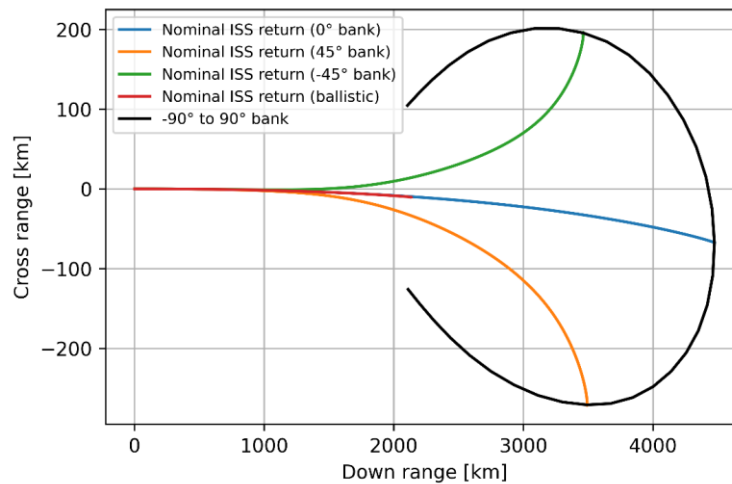
EURASTROS capsule design and re-entry analysis

Figure 5: Cross range for ISS return trajectories. The black line denotes splashdown locations for bank angles in the range.

4. Aerothermal Loads

During the re-entry of any space vehicle, high mechanical and thermal loads do occur. For a comprehensive analysis of the loads, the attitude and the dynamical behavior of a space vehicle, a large number of numerical simulations is necessary to optimize the mechanical design and the heat shield design in combination with the safety of the crew. However, the generation of a complete aerothermodynamic database (ATDB) is a time-consuming process.

For the initial design of the capsule only a few numerical simulations are considered crucial. The coefficients of lift and drag during the hypersonic flight phase which are important for the down range and the cross range of the capsule can be determined with high accuracy employing simple engineering models. However, in order to justify this expectation, the flight condition of peak dynamic pressure which coincides with maximum deceleration on the nominal trajectory was simulated employing the CFD solver TAU [6]. Since only a steady state result was obtained, only the force coefficients and the momentum coefficient can be obtained from the simulation but not the dynamic derivatives which are important for flight stability. This is considered sufficient for the time being due to the long-time experience with the selected Apollo type shape.

The flight condition with the highest thermal load is named 'Peak Heating'. The peak heating conditions on the nominal trajectory as well as for an emergency trajectory with ballistic entry were investigated. For these conditions, the spatial distribution of the surface heat fluxes as well as the corresponding surface temperatures are of particular interest. The maximum surface temperature is important for the selection of the material of the thermal protection system. The thickness of the thermal protection system must be derived based on the integrated heat load during flight. The two CFD simulations performed within this study are not suitable for an optimized design of the thermal protection system. However, they can be used to scale e.g. Fay-Riddell based stagnation point heat fluxes along the trajectory for an initial estimate of the integrated heat load to allow for a first assessment of the design of the thermal protection system [13]. The inflow conditions for the above mentioned three flight conditions which were investigated in detail by CFD are listed in Table 1.

Table 1: Trajectory points for nominal (lifting) and off-nominal (ballistic) return from ISS investigated with detailed CFD.

Flight mode	Condition	Altitude [km]	Ma	u_∞ [m/s]	p_∞ [Pa]	T_∞ [K]	ρ_∞ [kg/m³]
Lifting	Peak dynamic pressure	40.7	6.8	2162	254	253	0.0035
Lifting	Peak heating	67.7	24.2	7269	6.5	224	0.0001
Ballistic	Peak heating	53.8	19.6	6363	46	261	0.0006

The initial numerical grid for the CFD simulations resolves the flow domain with 2.4 million grid points. The surface normal resolution of the grid varies between 1.2×10^{-6} m on the windward side and 8×10^{-5} m on the lee side of the capsule. Hence, the normal resolution of the grid is of the order of the local mean free path length for all simulations. The boundary layer close to surface is resolved with 40 structured grid layers to allow for the determination of the surface heat flux with high accuracy. For all simulations, the grid was adapted several times based on Mach number

Marquardt, Fertig, Reimer, Gülhan

gradients and pressure gradients for the specific flight conditions to ensure a proper resolution especially of the bow shock. In each adaptation step the grid point number was increased by 15%. After 4 to 5 adaptation steps, the change of the surface heat fluxes between successive adaptation steps seemed sufficiently low to conclude that the obtained results are grid independent. Therefore, the final results shown below are obtained on grids with 4.2 million to 4.9 million grid points.
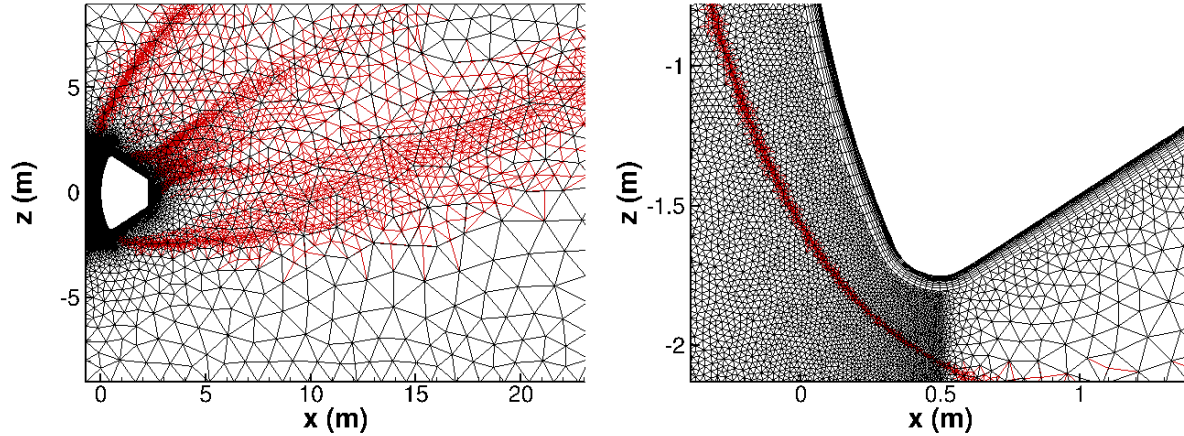

Figure 6: Initial (black) and final grid (red) for the peak dynamic pressure flight condition at Mach number 6.8 obtained after 4 adaptation steps. The plot on the left shows an overview of the flow field around the capsule. The plot on the right shows the grids in the vicinity of the shoulder more detailed.

Exemplarily, the initial and the final grid used for the simulation at Mach number 6.8 are shown in Figure 6. The plots show the grid lines in the symmetry plane. The initial grid is plotted in black, the final grid obtained after four adaptation steps is plotted in red. The plot on the left shows an overview of the flow domain around the capsule. Note that the grid dimensions are 45.7 m $\times$ 9 m $\times$ 18 m in *x*, *y* and *z* direction, respectively, to prevent from influences of the boundary conditions on the simulation results. It can be seen that the grid adaptation process improves not only the grid resolution upstream of the vehicle but also in the wake. The plot on the right shows the symmetry plane of the two grids in the vicinity of the shoulder of the capsule. The structured part of the grid in the vicinity of the surface can be recognized. Moreover, the red grid lines show the refinement of the grid in the shock layer. For all cases radiation equilibrium at the surface was assumed employing the emission coefficient $\varepsilon = 0.8$.

The peak dynamic pressure condition at Mach number 6.8 is associated with a maximum temperature of about 2000 K in the flow field. Hence, the perfect gas assumption is not suitable. However, due to the relatively high pressure of up to 15387 Pa and the expectation of a low degree of dissociation in the flow, local thermodynamic equilibrium was assumed. Under this assumption TAU employs an equilibrium database for the conversion between primitive (p, v, T) and conservative quantities $(\rho, \rho v, \rho e)$. Moreover, viscous transport coefficients are stored in this database as well. The database which is created in a pre-processing step resolves the thermodynamic quantities with at least 1000 data points. This means that e.g. the temperature which ranges between 10 K and 5000 K is resolved with $\Delta T = 5$ K. Laminar transport coefficients are computed employing the approach of Hirschfelder et al. [8][3]. For this flight condition, fully turbulent surface boundaries are assumed. Hence, at all viscous surfaces smooth turbulent boundary conditions are applied. The turbulence is modelled employing the Menter SST model with the model coefficients as from 2003 [9]. Numerical results for the flow field and the surface are shown in Figure 7. The plot on the left shows the temperature distribution in the symmetry plane using pseudo colors together with stream traces plotted in black. The shock structure is indicated by the sudden temperature increase. The plot on the right shows the pressure distribution for positive *y* and the heat flux distribution together with stream traces for negative *y*.
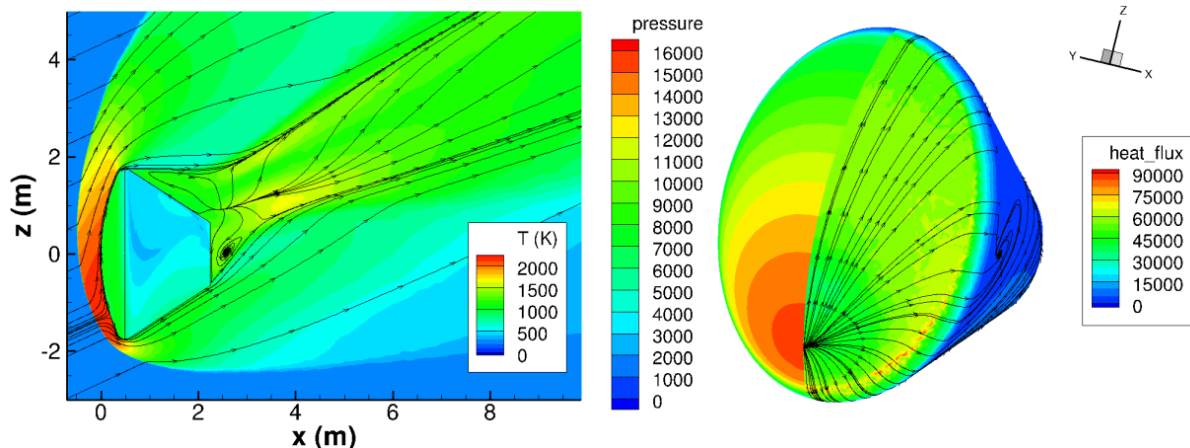
EURASTROS capsule design and re-entry analysis

Figure 7: The plot on the left shows the temperature distribution in the symmetry plane together with stream traces for the peak dynamic pressure flight condition at Mach number 6.8. The plot on the right shows the pressure distribution for positive y and the heat flux distribution together with stream traces for negative y.

The aerodynamic coefficients are determined using the reference length $l_{\mathrm{ref}} = d_{\mathrm{ref}} = 3.5$ m and the reference area $A_{\mathrm{ref}} = \pi/4 \ d_{ref}^2 = 9.621$ m^2. With these values the obtained force coefficients are $c_x = 1.2805$, $c_z = 0.1015$, $c_L = -0.4492$ and $c_D = 1.2035$ for the axial force coefficient, the normal force coefficient, the coefficient of lift and the coefficient of drag, respectively. The moment coefficient is $c_m = -0.0761$. The negative moment coefficient at positive angle of attack indicates statically stable behavior.

Laminar flow was assumed for the peak heating cases. Due to the higher velocities and temperatures, chemical nonequilibrium accounting for the species N_2, O_2, NO, N and O is considered in the simulations. The reaction rates are computed following Gupta et al. [5]. The laminar viscous transport coefficients were determined following Hirschfelder et al. [8], [3]. The usual design assumption, i.e. fully catalytic boundary conditions were applied at the surface. Numerical results for the lifting peak heating flight case at Mach number 24.2 are shown in Figure 8. The plot on the left shows the temperature distribution and stream traces in the vicinity of the capsule in the symmetry plane. The plot on the right shows the pressure and the heat flux distributions on the surface. The maximum pressure and the maximum heat flux at the surface for this flight condition are 5149 Pa and 1.02 MW/m², respectively. For this case the heat flux obtained at the center line might be more important to allow for scaling of the Fay-Riddell heat flux along the trajectory. The surface heat flux obtained at $(x, y, z) = (0, 0, 0)$ is $\dot{q}_{\mathrm{center}} = 385.6$ kW/m². Hence, one obtains the fraction $\dot{q}_{\mathrm{max}}/\dot{q}_{\mathrm{center}} = 2.65$.
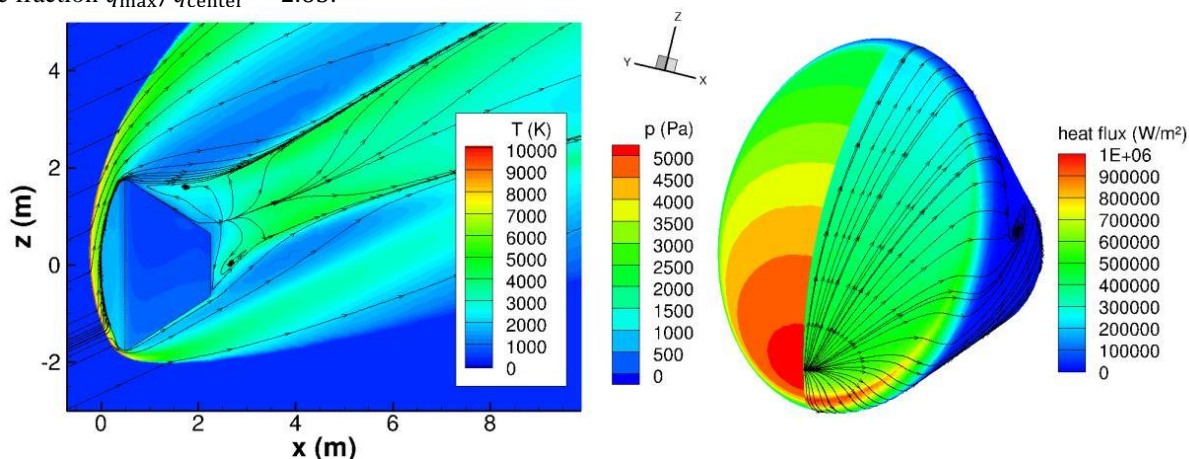

Figure 8: The plot on the left shows the temperature distribution in the symmetry plane together with stream traces for the peak heating flight condition for lifting entry at Mach number 24.2. The plot on the right shows the pressure distribution for positive y and the heat flux distribution together with stream traces for negative y.
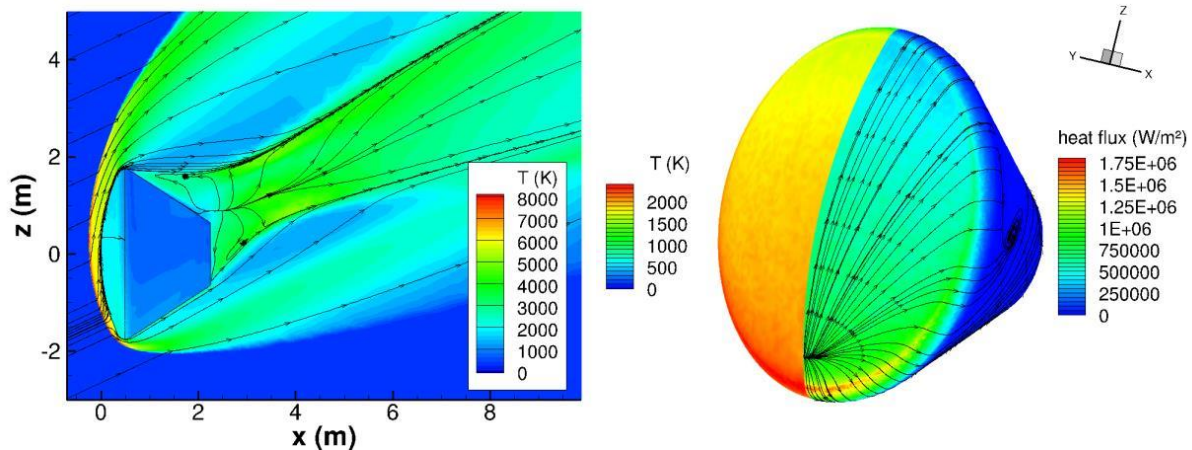
Marquardt, Fertig, Reimer, Gülhan

Figure 9: The plot on the left shows the temperature distribution in the symmetry plane together with stream traces for the peak heating flight condition for ballistic entry at Mach number 19.6. The plot on the right shows the temperature distribution for positive y and the heat flux distribution together with stream traces for negative y.

The numerical results for the peak heating condition of the emergency, ballistic entry trajectory is shown in Figure 9. The plot on the left shows the temperature distribution in the symmetry plane using pseudo colors together with stream traces plotted in black. Due to the lower flight velocity, the maximum temperature obtained in the flow field is significantly lower compared with the peak heating case for lifting entry. Since the peak heating condition arises at lower altitude for the ballistic case the surface heat flux becomes significantly larger as can be seen from the plot on the right. The plot shows the temperature distribution for positive y and the heat flux distribution together with stream traces for negative y. The maximum heat flux obtained for the peak heating condition at $Ma = 19.6$ is 1.76 MW/m². Based on the radiation equilibrium boundary condition with emissivity $\varepsilon = 0.8$ the corresponding maximum surface temperature is 2497 K. This temperature must not be higher than the maximum use temperature of the outer material of the thermal protection system at the shoulder of the capsule.

5. Capsule Structure and TPS Design

5.1 TPS material

As the baseline material for the TPS investigations, the low-density ablator material ZURAM® was selected based on previous development experience and experimental test campaigns. ZURAM® is a lightweight ablator based on a commercially available rigid carbon fiber preform which is infiltrated with a nano-porous phenolic resin. The production process has been developed over several years and a very stable level of material quality has been established. The material is fully characterized and a large data base from testing in arc-heated wind tunnels was established. In terms of performance, the material is comparable to competitor materials as ASTERM or PICA, so it is quite representative to select this material for the pre-development investigations presented here.

5.2 Capsule structure

With regard to the capsule structure an assumption was made for the basic structural concept, based on previous experience from the BERT study [12], but also based on existing examples e.g. the ORION structural concept. Since the outer shape of the capsule (OML) was given as in Figure 1, it was assumed that the capsule structure follows this shape with a given offset to accommodate the TPS and external stiffeners as well as equipment.
The main engineering assumptions considered for the design of the EURASTROS capsule structure are:
- The structural pressure vessel was assumed to consist of a cylindrical part with horizontal floor and a conical part on top.
- Offset of constant value to the inside of the OML to be available for TPS and stiffeners to form the structural pressure vessel of the capsule. The offset value was set at 100 mm fixed.
- The pressure vessel was supposed to feature stiffeners on the outside of the vessel.
- The stiffeners were assumed as orthogrid on the conical part and on the cylindrical part.
- Manufacturing was supposed to be done by friction stir welding mainly.
The initial structural concept of the capsule is depicted in Figure 10.
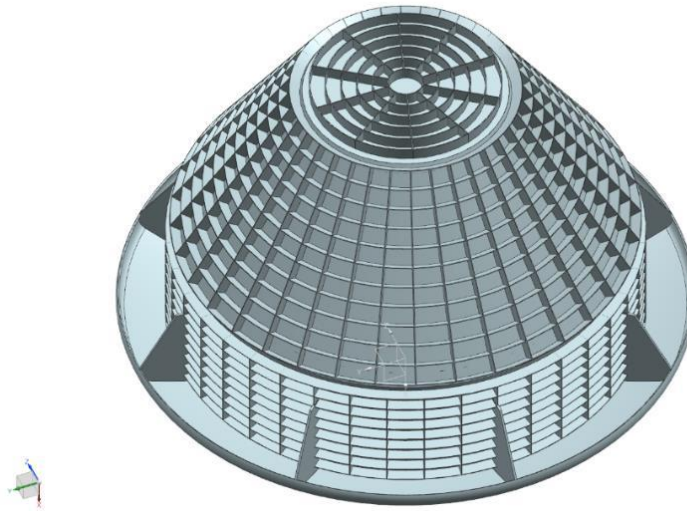
EURASTROS capsule design and re-entry analysis

Figure 10: Capsule structure outside view.

As for the mechanical loads that were to be investigated in this early phase, two load cases were defined. First, it was the pressure difference between capsule internal and external vacuum, second, it was the deceleration load due to the aerodynamic loads during re-entry as a result of the trajectory analysis showing that the launch abort from 250 km altitude creates the highest decelerations.

Table 2: Load cases for mechanical design.

Load	Value	Unit
Pressure difference Internal/external	1	bar
Deceleration	22	g

From the CAD model an FEM model was created and analyzed for these two load cases. The analysis results showed that the differential pressure load case is the dominating one for the assumptions made. In Figure 11 a result of the stress distribution is depicted showing the situation around the top cover where stresses are the highest. The wall thickness of the stiffeners was treated as a variable parameter to do some optimization. In general, it was found that the stress peaks are occurring at the top edges of the stiffeners and that the situation can be handled quite well by adjusting the individual geometry of the items. The resulting total mass of the structure was 792 kg.
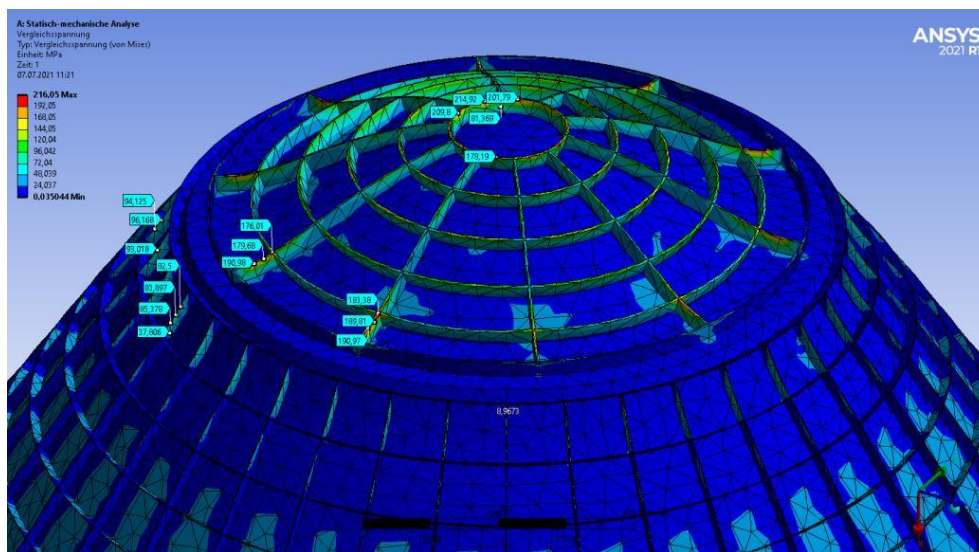

Figure 11: Stress distribution on the capsule top.

Marquardt, Fertig, Reimer, Gülhan

5.3 TPS sizing

In terms of the TPS sizing, an initial thickness of constant 100 mm was assumed to be available for the ablator material outside of the capsule structure. In the following, three different re-entry trajectories were considered for the actual sizing:

- ISS nominal return
- ISS ballistic return
- Ballistic launch abort from 250 km

For each of these, the trajectory data was available in terms of stagnation heat flux density over time and also in terms of heat flux distribution over the surface of the capsule at selected points of time.
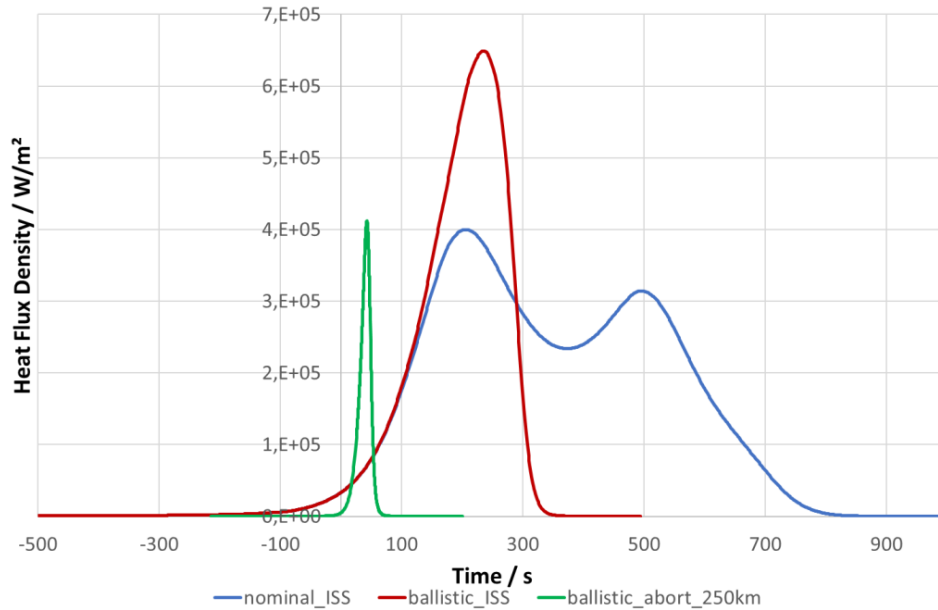

Figure 12: Sizing trajectories for TPS.

Figure 12 shows the transient heat flux profiles for the trajectories. For the TPS sizing, there are two main aspects to be considered. One is the issue of total recession of the ablator material, the second is the thermal insulation of the TPS material to protect the capsule structure. In terms of the sizing for recession, the required thickness values were calculated to be as given in Table 3, considering the high values for the leading edge as shown in Figure 8.

Table 3: Results of TPS sizing for recession.

Recession [mm]	Nominal ISS	Ballistic ISS	Abort 250 km
Stagnation	2.8	2.4	0.18
Leading Edge	15.2	9.6	

Concerning the sizing of the TPS with regard to the insulation of the capsule, transient thermal FEM analyses were carried out. The sizing criterion was a structure temperature of 100°C that was not to be surpassed. The resulting thickness values were calculated to be as given in Table 4.

Table 4: Results of TPS sizing for thermal insulation.

	Front Shield	Backshell
Thickness [mm]	68	44

Summarizing the TPS sizing, it can be said, that a thickness of 70 mm is required for thermal insulation and that the recession is not a sizing issue. The assumed geometric volume of total 100 mm is sufficient to accommodate the layer of ablator material.

The important interface elements of the capsule are the following:

- Mechanical interface to service module
- Electrical interface to service module
- Docking interface to space station

The mechanical interface to the service module is considered as a new development of high level of technical difficulty. Such items posed a great challenge in the development of the ORION heat shield. Therefore, it is anticipated that also for this concept a special solution needs to be developed with regard to the materials applied in the heat shield where the mechanical interface to the capsule is located. The docking adapter to the ISS is a standard piece of equipment which needs adaptation to the specific capsule requirements. Also, the electrical interfaces are regarded as available technology.

5.4 Internal volume distribution and mass considerations

An engineering concept was drawn up with regard to the distribution of the internal masses in terms of crew seating and equipment (Figure 13). The exercise was done to determine if it is possible to adjust the center of gravity in the way as it was foreseen by the baseline system considerations. The masses were calculated either via sizing effort, as for the TPS, or via comparison with previous work (e.g. BERT study). The resulting top-level mass table is presented in Table 5. A detailed mass breakdown of the capsule is given in Table 6.
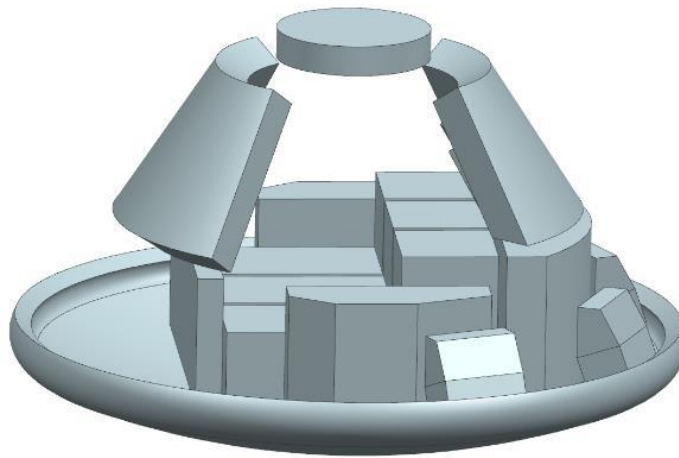

Figure 13: Concept of internal mass distribution in the capsule. Front TPS shown for orientation purpose.

Table 5: Capsule top-level mass breakdown.

Component	Mass [kg]
Structure	792
TPS	673
Equipment	2731
Crew (seats)	820
Total	**5016**

Marquardt, Fertig, Reimer, Gülhan

Table 6: Detailed capsule mass breakdown.

Element	Mass [kg]	Margin	Mass incl. Margin [kg]
Structure	689	15%	792
Front TPS	275	10%	303
Back TPS	336	10%	370
Crew	272	10%	299
Crew Items	474	10%	521
TCS	298	15%	343
ECLSS	298	15%	323
Power/Batteries	281	15%	233
Harness	123	15%	142
Data management	182	15%	209
Positioning	59	15%	68
Communication	76	15%	87
Propulsion	161	15%	185
Propellant	75	15%	86
Landing	593	15%	682
Docking	324	15%	373
Total			**5016**

6. Summary and Conclusions

In this study, the capsule of the EURASTROS study was analyzed. The capsule shape is derived from the Apollo shape, scaled down to 72% of its original volume to accommodate 2-3 astronauts. The static stability, nominal center of gravity location and aerodynamic coefficients were analyzed using the modified Newton method. To determine the design loads of the capsule, re-entry trajectories were calculated for ISS return with nominal (lifting) and off-nominal (ballistic) re-entry. The capsule experiences $2g$ deceleration for nominal and $8g$ deceleration for off-nominal ISS return. Much higher loads occur for launch abort. A generic abort case was defined that leads to $21.8g$ during re-entry. Additionally, the abort trajectory exhibits the maximum dynamic pressure of the investigated trajectories. The pressure distribution on the front shield, calculated using the modified Newton method, is used for the structural design of the capsule.

For a detailed aerothermal analysis, the trajectory points for peak dynamic pressure during nominal re-entry and the points of peak heating during nominal and off-nominal re-entry were chosen. The flow was analyzed using high resolution numerical simulations that included real gas effects in all cases and additional chemical non-equilibrium in the peak heating cases. The simulations confirmed static stability and the validity of the approximate aerodynamic coefficients from the modified Newton method, that are within 4% to the simulation. The peak heat flux occurs close to the shoulder of the capsule and reaches values of 1.02 MW/m² during nominal and 1.76 MW/m² during off-nominal re-entry.

The capsule is designed as a highly integrated metallic structure consisting of a cylindrical part with horizontal floor and a conical part on top, reinforced with orthogrid stiffeners on the outside of the pressure vessel. Two load cases, i.e., pressure difference between capsule internal and outside vacuum, and deceleration load during re-entry, were investigated via FEM. The analysis results showed that the differential pressure load case is the dominating one for the assumptions made. The resulting total mass of the structure is 792 kg. For the design of the thermal protection system, recession and thermal insulation were considered. The analysis showed that for thermal insulation a thickness of 70 mm is required for the front shield. The maximum recession, occurring for nominal ISS return, is 15.2 mm. The mass of the TPS was estimated as 673 kg resulting in a total mass of the capsule of 5016 kg.

The analysis of the re-entry trajectories assumed flight at a prescribed angle of attack. For future studies, the re-entry trajectories can be improved by using a more detailed aerodynamic database. The present study is focused on statically stable flight at hypersonic Mach numbers. The transonic region including parachute deployment should be addressed in a future study that also includes dynamic stability. Further investigations should be carried out on important interface elements of the capsule, e.g. the mechanical interface to the service module that poses great challenges for the development of the heat shield.

References

[1] Bergmann, K., Marquardt, P., Dietlein, I.; EURASTROS ascent trajectory and abort analysis, *EUCASS-3AF Conference*, Lille, France, 2022.

[2] Braukhane, A., Plebuch, A., Renk, T.; EURASTROS demonstration plan and cost analysis, *EUCASS-3AF Conference*, Lille, France, 2022.

[3] Fertig M., Dohr A. and Frühauf H.H., "Transport Coefficients for High Temperature Nonequilibrium Air Flows", AIAA Journal of Thermophysics and Heat Transfer, vol. 15, no. 2:pp. 148–156, Apr. 2001.

[4] Gülhan, A., Weihs, H., Sippel, M., Marquardt, P., Wolf, M., Plebuch, A., Fröbel, L., Lassmann, J.; An Overview of the EURASTROS Study, *EUCASS-3AF Conference*, Lille, France, 2022.

[5] Gupta, R. N. and Yos, J. M. and Thomson, R. A. and Lee, K.-P., "A Review of Reaction Rates and Transport Properties for an 11-Species Air Model for Chemical and Thermal Nonequilibrium Calculations to 30000K", Reference Paper 1232, NASA, 1990.

[6] Hannemann K., Martinez-Schramm J., Wagner A., Karl S. and Hannemann V., "A Closely Coupled Experimental and Numerical Approach for Hypersonic and High Enthalpy Flow Investigations Utilising the HEG Shock Tunnel and the DLR TAU Code", Tech. Rep. RTO-EN-AVT-186, German Aerospace Center, DLR, 2010.

[7] Heidrich, C. R., Braun, R. D., „Ballistic Reentry of Lifting Capsules at Earth Using Bank Rate Modulation", AIAA SPACE Forum, 2017.

[8] Hirschfelder J.O., Curtiss C.F. and Bird R.B.: "Molecular Theory of Gases and Liquids", John Wiley & Sons, New York, 1954.

[9] Menter F.R., Kuntz M. and Langtry R., "Ten Years of Industrial Experience with the SST Turbulence Model", Turbulence, Heat and Mass Transfer, Vol. 4, pp. 625–632, 2003.

[10] NASA, "ISS Crew Transportation and Services Requirements Document", CCT-REQ-1130 (Rev. E-1), 2016.

[11] Plebuch, A., Marquardt, P., Wolf, M.; System design of EURASTROS reference configurations and mission, *EUCASS-3AF Conference*, Lille, France, 2022.

[12] Sippel, M., Dietlein, I., Hanowski, N., Romberg, O., Schubert, D., Seboldt, W., Weihs, H., "Bemannter Europäischer Raum-Transport", SART TN-007/2008, 2008

[13] Tran, Ph., Paulat, J. C., Boukhobza, P., „Re-entry Flight Experiments Lessons Learned – The Atmospheric Reentry Demonstrator ARD", Technical Report, EADS ST, 2007.